Research Article | Vol. 24, No. 22 | 31 Oct 2016 | OPTICS EXPRESS 25154

Optics EXPRESS

Light scattering by oblate particles near planar interfaces: on the validity of the T-matrix approach

AMOS EGEL,[1,2,*] DOMINIK THEOBALD,[1] YIDENEKACHEW DONIE,[1,2] ULI LEMMER,[1,2] AND GUILLAUME GOMARD[1,2]

[1]*Light Technology Institute, Karlsruhe Institute of Technology, Engesserstr. 13, 76131 Karlsruhe, Germany*
[2]*Institute for Microstructure Technology, Karlsruhe Institute of Technology, Hermann-von-Helmholtz-Platz 1, 76344 Eggenstein-Leopoldshafen, Karlsruhe, Germany*
[*]*amos.egel@kit.edu*

Abstract: We investigate the T-matrix approach for the simulation of light scattering by an oblate particle near a planar interface. Its validity has been in question if the interface intersects the particle's circumscribing sphere, where the spherical wave expansion of the scattered field can diverge. However, the plane wave expansion of the scattered field converges everywhere below the particle, and in particular at the planar interface. We demonstrate that the particle-interface scattering interaction is correctly accounted for through a plane wave expansion in combination with Fresnel reflection at the planar interface. We present an in-depth analysis of the involved convergence mechanisms, which are governed by the transformation properties between spherical and plane waves. The method is illustrated with the cases of spherical and oblate spheroidal nanoparticles near a perfectly conducting interface, and its accuracy is demonstrated for different scatterer arrangements and materials.

OCIS codes: (290.5850) Scattering, particles; (290.5825) Scattering theory; (240.0240) Optics at surfaces; (250.5403) Plasmonics.

References and links

1. L. Novotny and N. van Hulst, "Antennas for light," Nat. Photonics **5**(2), 83–90 (2011).
2. Y.-J. Lee, S.-H. Kim, J. Huh, G.-H. Kim, Y.-H. Lee, S.-H. Cho, Y.-C. Kim, and Y. R. Do, "A high-extraction-efficiency nanopatterned organic light-emitting diode," Appl. Phys. Lett. **82**(21), 3779–3781 (2003).
3. G. Gomard, J. Preinfalk, A. Egel, and U. Lemmer, "Photon management in solution-processed organic light-emitting diodes: a review of light outcoupling micro- and nanostructures," J. Photon. Energy **6**(3), 030901 (2016).
4. P. C. Waterman, "Matrix formulation of electromagnetic scattering," Proc. IEEE **53**(8), 805–812, (1965).
5. M. Mishchenko, "T-matrix computations of light scattering by nonspherical particles: a review," J. Quant. Spectrosc. Radiat. Transf., **55**(5), 535–575, (1996).
6. N. G. Khlebtsov, "T-matrix method in plasmonics: An overview," J. Quant. Spectrosc. Radiat. Transf. **123**, 184–217, (2013).
7. G. Kristensson, "Electromagnetic scattering from buried inhomogeneities–a general three-dimensional formalism," J. Appl. Phys. **51**(7), 3486 (1980).
8. G. Videen, "Light scattering from a sphere on or near a surface," J. Opt. Soc. Am. A **8**(3), 483 (1991).
9. G. Videen, "Light scattering from a sphere on or near a surface: errata," J. Opt. Soc. Am. A **9**(5), 844–845 (1992)
10. D. W. Mackowski, "Exact solution for the scattering and absorption properties of sphere clusters on a plane surface," J. Quant. Spectrosc. Radiat. Transf. **109**(5), 770–788 (2008).
11. A. Egel and U. Lemmer, "Dipole emission in stratified media with multiple spherical scatterers: enhanced outcoupling from OLEDs," J. Quant. Spectrosc. Radiat. Transf. **148**, 165–176 (2014).
12. A. Doicu, Y. A. Eremin, and T. Wriedt, "Convergence of the t-matrix method for light scattering from a particle on or near a surface," Opt. Commun., **159**(4),266–277 (1999).
13. M. I. Mishchenko, G. Videen, V. A. Babenko, N. G. Khlebtsov, and T. Wriedt, "T-matrix theory of electromagnetic scattering by particles and its applications: a comprehensive reference database," J. Quant. Spectrosc. Radiat. Transf. **88**(1–3), 357–406 (2004).
14. For a collection of computer codes, see for example: www.scattport.org.
15. R.H.T. Bates, "Analytic constraints on electromagnetic field computations," IEEE Trans. Microwave Theory Tech. **23**(8), 605–623 (1975).
16. T. Hansen, and A. D. Yaghjian, *Plane-wave theory of time-domain fields: near-field scanning applications* (IEEE Press, 1999).

#274060 http://dx.doi.org/10.1364/OE.24.025154
Journal © 2016 Received 19 Aug 2016; revised 11 Oct 2016; accepted 11 Oct 2016; published 19 Oct 2016

Optics EXPRESS

17. C. Cappellin, O. Breinbjerg, and A. Frandsen, "Properties of the transformation from the spherical wave expansion to the plane wave expansion," Radio Sci. **43**(1), RS1012 (2008).
18. K. A. Fuller, "Optical resonances and two-sphere systems," Appl. Opt. **30**(33), 4716–4731 (1991).
19. D. W. Mackowski and M. I. Mishchenko, "Calculation of the T matrix and the scattering matrix for ensembles of spheres," J. Opt. Soc. Am. A **13**(11), 2266 (1996).
20. A. Boström, G. Kristensson, and S. Ström, "Transformation properties of plane, spherical and cylindrical scalar and vector wave functions," in *Acoustic, Electromagnetic and Elastic Wave Scattering, Field Representations and Introduction to Scattering*, V. V. Varadan, A. Lakhtakia, and V. K. Varadan, eds. (Elsevier, 1991).
21. D. Ngo, G. Videen, and R. Dalling, "Chaotic light scattering from a system of osculating, conducting spheres," Phys. Lett. A **227**(3), 197–202 (1997)
22. A. Doicu, T. Wriedt, and Y. A. Eremin, *Light Scattering by Systems of Particles* (Springer, 2006).
23. G. Videen, "Light scattering from a particle on or near a perfectly conducting surface," Opt. Commun. **115**(1), 1–7 (1995)
24. COMSOL Multiphysics, ver. 5.2, www.comsol.com.

1. Introduction

Many applications in nano optics rely on the interaction of light with wavelength scale particles near planar surfaces, for example plasmonic structures supported by a substrate [1], or scattering layers for light management in optoelectronic thin film devices, such as organic light emitting diodes [2, 3]. The T-matrix method [4–6], one of the most powerful tools for the modelling of light scattering by compact particles, has been adapted to include the scattering interaction between the particles and planar interfaces [7–11]. It relies on an expansion of the particle's scattered field in terms of outgoing spherical waves relative to the particle center.

However, this outgoing spherical wave expansion (SWE) is in general only valid outside the smallest sphere that includes the whole particle, whereas inside that sphere it may diverge. If an oblate particle is located near a planar surface, the surface intersects the particle's circumscribing sphere, see Fig. 1. Then, the SWE may not converge everywhere on the planar surface [12], which puts the general validity of the T-matrix approach for such systems into question. This apparent restriction might be one reason why, despite its numerous benefits [5], the T-matrix formalism is not employed more frequently in application-oriented studies of light scattering by photonic structures near interfaces.

The objective of the present paper is to demonstrate that the scattered field can be accurately computed using the T-matrix formalism - even if the circumscribing sphere and the planar surface intersect - thereby paving the way for a wider use of that method in the modelling of photonic structures supported by a substrate. The main steps in the line of argument are the following:

- First, we briefly summarize the general procedure for the computation of the scattered field of a particle near a planar surface (section 2). In order to evaluate the reflection from the surface, the SWE of the scattered field is temporarily transformed into a plane wave expansion (PWE) [7]. The whole approach thus depends on the validity of the PWE (and not of the SWE) at the planar surface.

- In section 3, we assess the validity of the scattered field's PWE. We conclude that it is valid even in the near field region of the particle where the outgoing SWE breaks down.

- A discussion of the convergence mechanism reveals that the truncation of the scattered field's PWE and the truncation of its SWE should not be chosen independently. For a fixed truncation multipole order of the SWE, the method can only provide accurate results if the PWE is truncated within a certain range of the in-plane wavenumber. Surprisingly, a larger PWE truncation wavenumber leads to a decrease in accuracy.

- The analysis is finally illustrated with two case studies: For the scattering of a plane wave by five spheres (treated as a single composite particle) near a perfectly conducting

Optics EXPRESS

substrate, the accuracy of the T-matrix formalism is examined by comparing the scattered field coefficients to the exact solution of that system (section 4). Finally, we give numerical results for an oblate spheroid near a planar surface and compare the computed near fields to results obtained with the finite element method (FEM) in section 5.

This paper does *not* cover the computation of the T-matrix for a given scattering particle. Instead, we use third-party code and algorithms to compute the T-matrix for the application examples discussed in sections 4 and 5, whereas in sections 2 and 3 we just assume that it is precisely known. Under that assumption, the scope of the analysis provided in this paper is not restricted to a certain class of particle shapes. It holds for particles with and without axial symmetry. In this spirit, we use the term "oblate particle" in the broadest possible sense for all objects that extend further into the lateral directions than into the direction orthogonal to the planar surface.

2. Particles near interfaces: the general procedure

Scattering by particles near planar interfaces has been well studied in the framework of the T-matrix formalism [7–11]. For the sake of clarity, we briefly summarize the general procedure, considering the following scattering configuration: A planar interface I at $z = z_\mathrm{I} < 0$ separates two regions of constant refractive index, n_0 in the upper region and n_1 in the lower region. For simplicity, we assume that these materials are linear, nonmagnetic and isotropic. A scattering particle S is located inside the upper region and its center coordinate coincides with the coordinate origin. We denote the volume occupied by the scatterer with V_S. The particle is illuminated by a monochromatic initial field (e.g., a plane wave, a Gaussian beam or the field of a point dipole source) with angular frequency ω. In the upper half space, we can write the total electric field as

$$\mathbf{E}(\mathbf{r}) = \mathbf{E}_0(\mathbf{r}) + \mathbf{E}_\mathrm{S}(\mathbf{r}) + \mathbf{E}_\mathrm{S}^\mathrm{R}(\mathbf{r}),$$

where the initial field $\mathbf{E}_0(\mathbf{r})$ solves Maxwell's equations for the half-space problem without the particle S, and the scattered field $\mathbf{E}_\mathrm{S}(\mathbf{r})$ as well as its reflection $\mathbf{E}_\mathrm{S}^\mathrm{R}(\mathbf{r})$ from the planar interface fulfill the Silver-Müller radiation boundary condition at infinity.

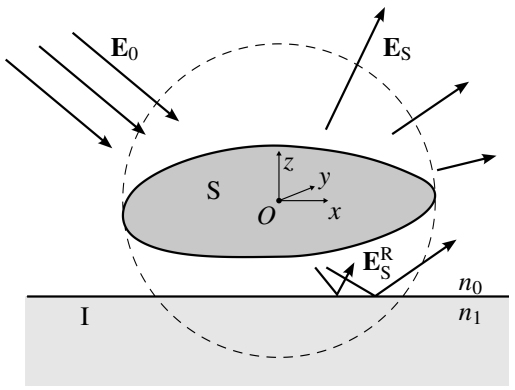

Fig. 1. Oblate scattering particle near a planar surface

In the T-matrix formalism, the incoming field $\mathbf{E}_\mathrm{in}$ at the particle is expanded in regular spherical vector wave functions, the $\mathbf{M}_n^{(1)}(\mathbf{r})$ (see appendix 6). It includes the initial field, and the reflection from its own scattered field at the interface I. We denote the coefficients of the incoming field

Optics EXPRESS

by a_n:

$$\begin{aligned}\mathbf{E}_{\text{in}}(\mathbf{r}) =& \mathbf{E}_0(\mathbf{r}) + \mathbf{E}_{\text{S}}^{\text{R}}(\mathbf{r}) \\ =& \sum_n a_n \mathbf{M}_n^{(1)}(\mathbf{r}).\end{aligned}$$

In this expansion, the summation runs over the following indices: the degree l and order m of the multipole, as well as the polarization p of the spherical wave. For the sake of a more concise notation, these indices are subsumed into a single index $n = (l, m, p)$.

Further, the scattered field is represented by an outgoing SWE:

$$\mathbf{E}_{\text{S}}(\mathbf{r}) = \sum_n b_n \mathbf{M}_n^{(3)}(\mathbf{r}). \tag{1}$$

Then, the T-matrix of the particle is defined as the linear operator that maps the incoming field coefficients a_n to the scattered field coefficients b_n,

$$b_n = \sum_{n'} T_{nn'} a_{n'}. \tag{2}$$

It incorporates the complete scattering behavior of the particle S. Efficient and accurate methods for the computation of the T-matrix have been proposed for a broad class of particles [13], and computer codes are freely available (for a collection, see [14]). In the present paper, we assume that the T-matrix is precisely known. In order to solve for the scattered field coefficients, one needs to first evaluate the incoming field coefficients,

$$a_n = a_{0,n} + a_{\text{S},n}^{\text{R}},$$

where $a_{0,n}$ and $a_{\text{S},n}^{\text{R}}$ are the coefficients of a regular SWE of the initial field and the reflected scattered field, respectively. Whereas $\mathbf{E}_0$ is known a priori, $\mathbf{E}_{\text{S}}^{\text{R}}$ and therefore the coefficients $a_{\text{S},n}^{\text{R}}$ depend on the scattered field coefficients. In order to evaluate $a_{\text{S},n}^{\text{R}}$, one proceeds as follows. First, the scattered field is expanded in terms of downwards propagating plane vector wave functions (see appendix 6), by replacing $\mathbf{M}_n^{(3)}$ in Eq. (1) with the right hand side of Eq. (11):

$$\mathbf{E}_{\text{S}}(\mathbf{r}) = \sum_{n'} \sum_j \frac{b_{n'}}{2\pi} \int_{\mathbb{R}^2} \frac{\mathrm{d}^2\mathbf{k}_\parallel}{k_z k} B_{n'j}(-k_z/k)\, \mathbf{E}_j^-(\kappa, \alpha; \mathbf{r})\, \mathrm{e}^{\mathrm{i}m'\alpha} \tag{3}$$

The above integral runs over all possible directions of downwards propagating and evanescent plane waves, each of which is characterized by its polarization j as well as the wavevector, expressed in cylindrical coordinates as (κ, α, k_z). Further, $k = n_0\omega/c$ denotes the wavenumber in the upper half space and $\mathbf{k}_\parallel = (k_x, k_y)$ stands for the in-plane components of the wavevector. For each partial plane wave in this expansion, the reflection from the interface is evaluated by means of the Fresnel reflection coefficient $\rho_j(\kappa)$ to yield

$$\mathbf{E}_{\text{S}}^{\text{R}}(\mathbf{r}) = \sum_{n'} \sum_j \frac{b_{n'}}{2\pi} \int_{\mathbb{R}^2} \mathrm{d}^2\mathbf{k}_\parallel \frac{\rho_j(\kappa)\, \mathrm{e}^{-2\mathrm{i}k_z z_1}}{k_z k} B_{n'j}(-k_z/k)\, \mathbf{E}_j^+(\kappa, \alpha; \mathbf{r})\, \mathrm{e}^{\mathrm{i}m'\alpha}. \tag{4}$$

The reflected partial plane waves are then transformed back into a regular SWE using Eq. (12). After integrating over α (using $\mathrm{d}^2\mathbf{k}_\parallel = \mathrm{d}\alpha\kappa\mathrm{d}\kappa$), one obtains

$$\mathbf{E}_{\text{S}}^{\text{R}}(\mathbf{r}) = 4 \sum_n \sum_{n'} \sum_j \delta_{mm'} b_{n'} \int_0^\infty \mathrm{d}\kappa \frac{\kappa\rho_j(\kappa)\, \mathrm{e}^{-2\mathrm{i}k_z z_1}}{k_z k} B_{n'j}(-k_z/k)\, B_{nj}^\dagger(k_z/k)\, \mathbf{M}_n^{(1)}(\mathbf{r})$$

Optics EXPRESS

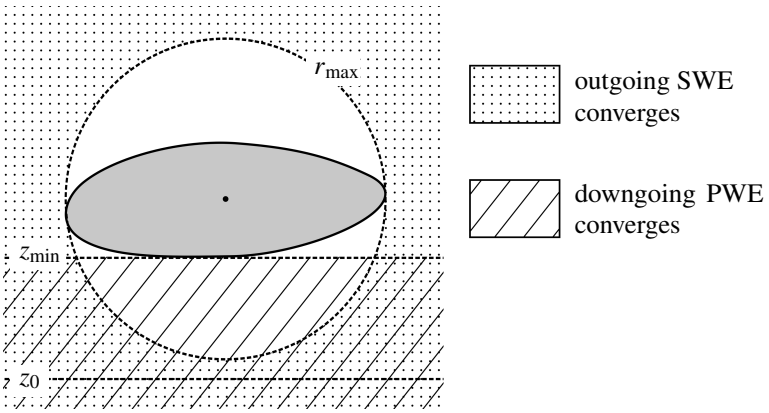

Fig. 2. The expansion of $\mathbf{E}_{\mathrm{S}}(\mathbf{r})$ in outgoing spherical waves is valid for $r > r_{\max}$. The expansion in downgoing plane waves is valid for $z < z_{\min}$. In the dashed white region, the expansion in downgoing plane waves is thus valid, even if the expansion in outgoing spherical waves does not converge. The plane $z = z_0$ is inside the domain of validity for both expansions.

which can be rewritten as

$$\mathbf{E}_{\mathrm{S}}^{\mathrm{R}}(\mathbf{r}) = \sum_n a_{\mathrm{S},n}^{\mathrm{R}} \mathbf{M}_n^{(1)}(\mathbf{r})$$

for

$$a_{\mathrm{S},n}^{\mathrm{R}} = \sum_{n'} W_{nn'}^{\mathrm{R}} b_{n'} \tag{5}$$

with

$$W_{nn'}^{\mathrm{R}} = 4 \sum_j \delta_{mm'} \int_0^\infty \mathrm{d}\kappa \frac{\kappa \rho_j(\kappa) \, \mathrm{e}^{-2\mathrm{i}k_z z_{\mathrm{I}}}}{k_z k} B_{n'j}(-k_z/k) \, B_{nj}^{\dagger}(k_z/k) \,. \tag{6}$$

Inserting Eq. (5) into Eq. (2) gives a set of self-consistent linear equations for the scattered field coefficients

$$b_n = \sum_{n'} T_{nn'} \left(a_{0,n'} + a_{0,n'}^{\mathrm{R}} + \sum_{n''} W_{n'n''}^{\mathrm{R}} b_{n''} \right), \tag{7}$$

the solution of which yields the scattered field according to Eq. (1).

3. Plane wave expansion of $\mathbf{E}_{\mathrm{S}}(\mathbf{r})$ in the near field

A key feature of the formalism described in section 2 is the temporary expansion of the scattered field in downgoing plane waves, which allows employing Fresnel's reflection formula in order to evaluate the response from the planar interface. In this section, we turn our attention to the domain of applicability of this expansion. In the case of spherical waves, it is a well known fact that the expansion in Eq. (1) is in general only valid outside the smallest circumscribing sphere with radius $r_{\max} = \max_{\mathbf{r} \in V_{\mathrm{S}}} r$ around the scatterer, whereas for $r < r_{\max}$ it does in general not converge [15]. However, although the PWE in Eq. (3) is constructed using the outgoing SWE, it turns out that the domains of validity for these expansions are *not* the same. To see this, it is instructive to think of the scattered field as the collective signal radiated by a current

Optics EXPRESS

density that is induced inside the scatterer S. For the moment, we are only interested in the direct scattered field $\mathbf{E}_\mathrm{S}(\mathbf{r})$ and not in the reflected field $\mathbf{E}_\mathrm{S}^\mathrm{R}(\mathbf{r})$, such that we can temporarily remove the interface I and think of the scatterer being embedded in an infinite homogeneous medium with refractive index n_0. In addition, we assume that at some plane defined by $z = z_0$ (with $z_0 < -r_\mathrm{max}$, see Fig. 2) the order of summation and integration in Eq. (3) can be interchanged:

$$\mathbf{E}_\mathrm{S}(\mathbf{r}) = \sum_j \int_{\mathbb{R}^2} \frac{\mathrm{d}^2\mathbf{k}_\parallel}{k_z k} \sum_{n'} \frac{b_{n'}}{2\pi} B_{n'j}(-k_z/k)\, \mathbf{E}_j^-(\kappa, \alpha; \mathbf{r})\, \mathrm{e}^{\mathrm{i}m'\alpha} \text{ for } z = z_0. \tag{8}$$

Note that the only difference between Eq. (8) and Eq. (3) is that the summation over n' has been written inside the integral. The above expression defines the so-called angular spectrum representation [16] of $\mathbf{E}_\mathrm{S}(\mathbf{r})$,

$$\mathbf{E}_\mathrm{S}(\mathbf{r}) = \int_{\mathbb{R}^2} \mathrm{d}^2\mathbf{k}_\parallel\, \mathbf{T}(\mathbf{k}_\parallel)\, \mathrm{e}^{\mathrm{i}\mathbf{k}^-\cdot\mathbf{r}} \tag{9}$$

with

$$\mathbf{T}(\mathbf{k}_\parallel) = \sum_j \sum_{n'} \frac{b_{n'}}{2\pi} \frac{B_{n'j}(-k_z/k)}{k_z k} \mathrm{e}^{\mathrm{i}m'\alpha} \hat{\mathbf{e}}_j. \tag{10}$$

In general, the angular spectrum representation (i.e., the PWE) is valid for all $z < z_\mathrm{min}$ where $z_\mathrm{min} = \min_{\mathbf{r}\in V_\mathrm{S}} z$ bounds the source region (i.e., the scattering particle S) from below. In particular, it is also valid in a part of the region inside the circumscribing sphere (see Fig. 2) where the outgoing SWE in general breaks down [17].

At first sight, this seems to be in conflict with the fact that the angular spectrum representation $\mathbf{T}(\mathbf{k}_\parallel)$ in Eq. (10) was derived starting from an outgoing SWE of $\mathbf{E}_\mathrm{S}(\mathbf{r})$. How is it possible that a finite expression (9) for $\mathbf{E}_\mathrm{S}(\mathbf{r})$ emerges from a diverging expression (1)? The reason for this apparent contradiction is related to the change in the order of integration and summation from Eq. (3) to Eq. (8). Whereas by assumption, this operation is justified for $z = z_0$, it is in general not allowed in the near field region, i.e. for $z \to z_\mathrm{min}$. There, the right hand side of Eq. (10) does not converge uniformly, but only point-wise to $\mathbf{T}(\mathbf{k}_\parallel)$.

In practice, the SWE is always truncated at a maximal multipole order l_trunc, and the PWE is truncated at a maximal in-plane wavenumber κ_trunc. Obviously, for a finite sum and a finite integral, the order of integration and summation plays no role. However, in order to achieve an accurate representation of the scattered near field in the region $z < z_\mathrm{min}$, we need to select the truncation parameters l_trunc and κ_trunc in the spirit of $\int \mathrm{d}\kappa \sum_n$ (as in Eq. (8)), rather than $\sum_n \int \mathrm{d}\kappa$ (as in Eq. (3)). That means, we need to make sure that the truncation multipole order l_trunc is chosen large enough such that for each $|\mathbf{k}_\parallel| \le \kappa_\mathrm{trunc}$ the angular power spectrum has converged to its true value. In contrast, if we select the truncation parameters the other way round, i.e., such that κ_trunc is large enough to make sure that for each $l \le l_\mathrm{trunc}$ the integral over κ has converged, the resulting field will exactly resemble the original SWE, and in particular show the same divergent behavior for $l_\mathrm{trunc} \to \infty$. As a consequence, we are facing the seemingly paradoxical situation that for a fixed truncation multipole order l_trunc, the calculated near field may be more accurate if a small cut-off wavenumber κ_trunc is chosen rather than a large one. This point will be further illustrated by the following case study, see section 4.1.

4. First case study: five dielectric spheres

We study the scattering of light at a chain of five identical dielectric spherical particles. This system is chosen because it allows for an exact solution, and at the same time it is a representative example of an oblate particle if the spheres are regarded as a single composite object. For that reason, it is an ideal test case for the formalism described in section 2.

Optics EXPRESS

The spheres have a refractive index $n_S = 2.4$ and radius R, and are located at $\mathbf{r}_i = (2(i-3)R, 0, 0)$, $i = 1, \ldots, 5$. The system is illuminated by a plane wave, polarized along the y-direction and propagating into the negative z-direction with a wavenumber $k = 1/R$ (i.e., each sphere has a dimensionless size parameter of $kR = 1$). First, we will examine the scattered near-field in the absence of a planar interface in order to demonstrate the validity of the plane wave representation in Eq. (8), and then consider the case for which spheres are located near a perfectly conducting substrate.

4.1. Five spheres in free space

The scattering problem can be exactly solved treating the spheres as individual scattering particles. Then, the scattered field is expressed by means of a SWE relative to each of the five sphere centers. The coefficients of that expansion can be constructed following, e.g., [18]. Because the circumscribing sphere is identical to the particle when individual spheres are considered, that representation of the fields converges everywhere outside the particles. This solution will serve us as an exact reference in the following analysis, see Fig. 3(A). Alternatively, one can treat the five spheres as a single, composite (i.e., non-connected) particle. Its T-matrix can then be constructed using the superposition T-matrix formalism [19].

It is important to note the difference between the two approaches that we are comparing: In the individual-particles picture, the scattered field is given by a sum of five expansions in spherical waves relative to the respective sphere centers. In the composite-particle picture, the scattered fields are *regrouped* into a single spherical wave expansion relative to the sphere in the middle of the chain. The difference between these approaches is an instructive illustration of the philosophy that underlies the T-matrix method in general: the whole particles' scattered field is represented in terms of spherical waves emerging from the particle center - although the actual source of radiation (the induced current distribution) is distributed over the whole particle volume.

Figure 3(B) shows the error of the scattered near field, which has been calculated according to Eq. (1) and Eq. (2) with a truncation of the SWE at a polar multipole order of $l_{\mathrm{trunc}} = 20$. It can be verified that the SWE of the scattered field in the composite-particle approach accurately resembles the exact near-field, except in the domain near to the coordinate origin, where it diverges. It is worth noting that the domain of convergence of Eq. (1) in fact overlaps the circumscribing sphere of the composite particle. It reaches down to the radius of the smallest sphere containing all singularities of the analytic continuation of the scattered field into the scattering particle (compare [15]), which are, in this example, located at the centers of the five spheres.

Figures. 3(C) and (D) show the error of the scattered field expressed in terms of a PWE. The coefficients of the PWE were calculated from the scattered field coefficients b_n of the composite particle using Eq. (8). For Fig. 3(C), the integral over the in-plane wavenumber was truncated at $\kappa_{\mathrm{trunc}} = 2k$, whereas for Fig. 3(D) $\kappa_{\mathrm{trunc}} = 50k$ was chosen. As expected, above the particles, the field diverges for both cases, because a downgoing PWE is in general only valid for $z < z_{\mathrm{min}}$. Below the spheres, the achieved accuracy differs, which is a consequence of the different truncation in-plane wavenumber of the PWE, respectively. In Fig. 3(C), the error of the scattered near-field is acceptable for all $z < z_{\mathrm{min}}$ (and partly even above). In contrast, Fig. 3(D) reveals that for large κ_{trunc}, the field inherits the divergent behavior near the coordinate from the SWE of the composite particle, compare Fig. 3(B).

This behavior could be expected with regard to the discussion presented in the last paragraph of section 3. We take a closer look at the plane wave spectrum for different truncation multipole orders in the SWE. Figure 4 shows the norm of the integrand of Eq. (9) for $\mathbf{r} = (0, 0, -1.5R)$, i.e., $\mathbf{T}(\kappa\hat{\mathbf{e}}_x)\exp(1.5\mathrm{i}k_z R)$, as a function of the in-plane wavenumber κ. Each line corresponds to a different truncation multipole order l_{trunc} up to which the sum over n was executed in the right hand side of Eq. (10). The solid black line depicts the exact spectrum, constructed from the

Optics EXPRESS

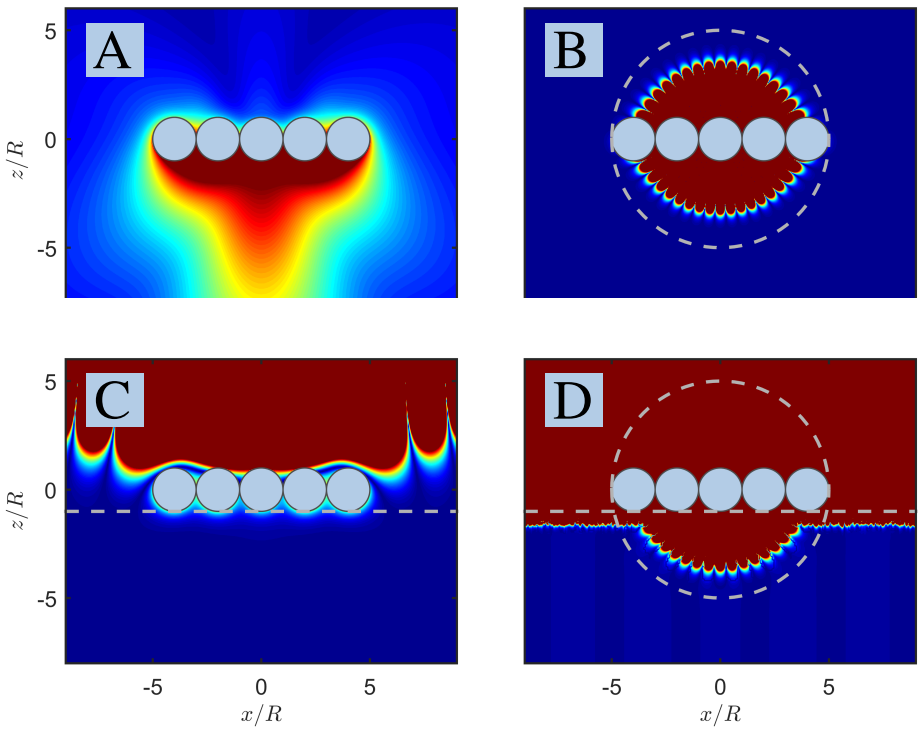

Fig. 3. Scattering of a downward propagating plane wave at five dielectric spheres in free space. **A:** The norm of the exact scattered near-field. **B:** Error of the field constructed with the superposition T-matrix for the composite particle, truncated at $l_{\text{trunc}} = 20$. **C:** Error of the field constructed with the superposition T-matrix, truncated at $l_{\text{trunc}} = 20$, then transformed into the angular spectrum representation, Eq. (8), truncated at $\kappa_{\text{trunc}} = 2\,k$. **D:** The same as C, but with $\kappa_{\text{trunc}} = 50\,k$. The dashed circles and lines indicate the boundary of the domains of validity for the SWE and the PWE, respectively. The color scale reaches from 0 (dark blue) to 0.8 (dark red).

reference solution. With growing l_{trunc}, the curves converge point-wise to the exact spectrum. For each curve, the spectral axis can be roughly divided in three domains: In the interval $[0, \kappa_1]$, the curve is in good agreement with the exact spectrum and deviates less than some specified tolerance (e.g., less than 5 %). This interval of convergency is followed by an interval $[\kappa_1, \kappa_2]$ in which the curve deviates strongly from the exact spectrum and takes huge values. Finally, for $\kappa > \kappa_2$, the curve drops to very small values (e.g., below 10^{-5}), as the suppression by the factor $\exp(-\mathrm{i}k_z z)$ becomes dominant, because $k_z = (k^2 - \kappa^2)^{1/2}$ is an imaginary quantity of growing modulus. The position of the interval $[\kappa_1, \kappa_2]$ thereby depends on the truncation multipole order and on the position where the field is evaluated. For growing l_{trunc}, the interval is shifted to higher κ, and at the same time the maximum of the curves in the interval of divergence grows to larger and larger values. This is why for field locations inside the circumscribing sphere of the scatterer, the curves do not converge uniformly to the exact spectrum, but only point-wise with respect to κ.

For the convergency in real space, these spectral regions have the following meaning: From the waves in the first interval, $[0, \kappa_1]$, the scattered near- and far-field can be constructed. The computed field approximates the exact field well if l_{trunc} was chosen large enough to allow

Optics EXPRESS

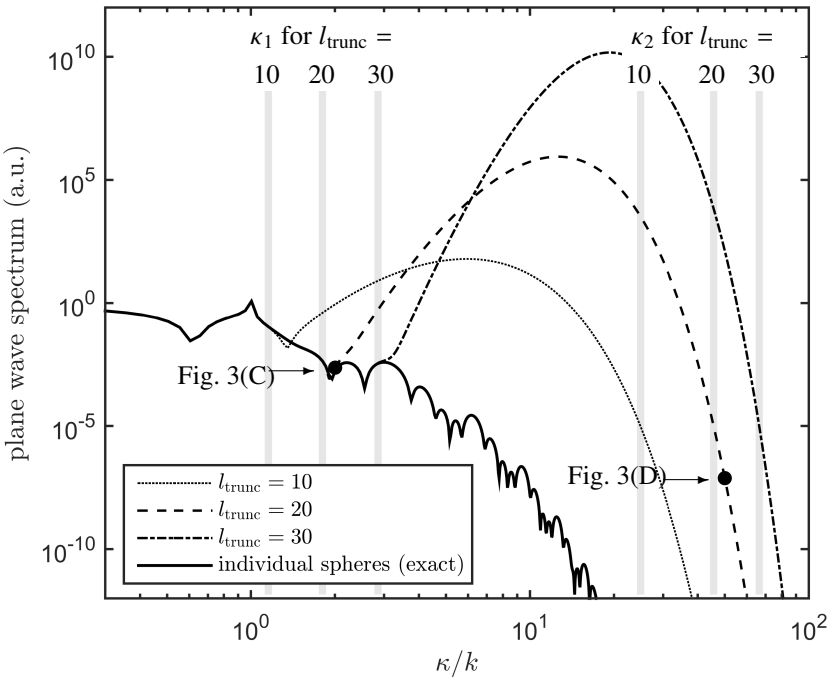

Fig. 4. Plane wave expansion of the scattered field for five spheres in free space. The y-axis shows the weight of the respective partial plane waves to the scattered electric field evaluated at $1.5R$ below the particle centers, $\left|\mathbf{T}\left(\kappa\hat{\mathbf{e}}_x\right)\exp(1.5\mathrm{i}k_z R)\right|$. The solid curve corresponds to the exact PWE constructed from the reference solution. The dashed, dotted and dash-dotted lines correspond to the PWE in the composite-particle approach for different truncation multipole orders l_{trunc} in the right hand side of Eq. (8). The vertical grey lines indicate the location of κ_1 and κ_2 for the respective truncation multipole orders. We have also marked the points up to which the PWE was considered in the evaluation of the scattered fields shown in Figs. 3(C) and (D), respectively, as black dots.

for a sufficiently high κ_1, such that all relevant evanescent waves are included. In contrast, the interval $[\kappa_1, \kappa_2]$ includes those evanescent waves that build up the divergent field inside the circumscribing sphere of the scatterer. If the PWE is truncated at $\kappa \geq \kappa_2$, it resembles the SWE up to the multipole order l_{trunc}. In particular, the so constructed field may diverge inside the circumscribing sphere of the scatterer, just as the SWE. The truncation parameters l_{trunc} and κ_{trunc} that were used for the construction of the fields displayed in Fig.s 3(C) and (D) are marked in Fig. 4. For the case of Fig. 3(C), κ_{trunc} corresponds to κ_1 whereas for Fig. 3(D), κ_{trunc} comes near κ_2. This explains, why Fig. 3(D) shows a divergent near-field below the particle, whereas the field in Fig. 3(C) is a good approximation to the exact field for all $z < z_{\text{min}}$. Note that if the test plane (in our case $z = -1.5R$) is shifted towards $z = 0$, the suppression factor $\exp(-\mathrm{i}k_z z)$ becomes weaker, and κ_2 grows to larger values. For that reason, Fig. 3(D) exhibits a large error for $z \gtrsim -1.5R$. There, κ_2 is larger than the chosen $\kappa_{\text{trunc}} = 50\,k$ of the PWE which thus has not yet converged to the field given by the SWE.

4.2. *Five spheres near a perfectly conducting substrate*

We now introduce the case of five spheres located near a planar interface which separates the upper half space with $n_0 = 1$ from a perfectly conducting substrate, with a distance of Δz

Optics EXPRESS

between the interface and the spheres, see Fig. 5. Accordingly, the initial field also includes the reflection of the incident plane wave with a reflection coefficient of $\rho_{\mathrm{TE}}(\kappa) = -1$. Again, there are different possible approaches to model that system. In the following, we will compare three solutions.

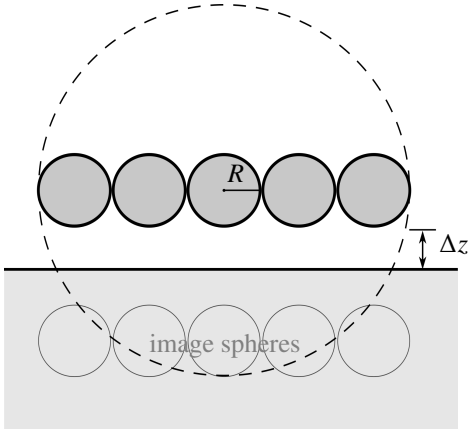

Fig. 5. Five dielectric spheres near a perfectly conducting substrate.

First, we model the spheres as individual particles and account for the particles-interface scattering by switching to the equivalent image particle problem (compare [8]) with ten individual spheres in free space, which can be solved with high precision [19]. For a perfectly conducting substrate, the image method is exact such that we can use it as a reference solution.

The second approach corresponds to the method described in section 2. We model the five spheres as a single composite particle through the superposition T-matrix. The particle/substrate interaction is accounted for through a PWE of the scattered field. For the numerical evaluation of the Sommerfeld integral in Eq. (6), we use the trapezoidal rule with a sampling of $10^{-4}k$ and a truncation scale κ_{trunc}. In the vicinity of the branch point at $\kappa = k$, we deflect the integral contour slightly into the negative imaginary for a better accuracy.

Finally, in the third approach, we again employ the image method but for the composite particle, i.e., solving a two-particle system. For small particle-interface distances, when the circumscribed spheres of the composite particle and of its image intersect, this method can in general not be expected to converge to the correct field.

We measure the accuracy of a computed solution by comparing the scattered field coefficients b_n to those of the exact reference solution, $b_{\mathrm{exact},n}$. For that purpose, we use the spherical vector wave addition theorem [20] to construct an outgoing SWE relative to the coordinate origin for the total scattered field of all five spheres. The relative error is defined as

$$\text{relative error} = \frac{\|\mathbf{b} - \mathbf{b}_{\mathrm{exact}}\|}{\|\mathbf{b}_{\mathrm{exact}}\|},$$

where $\|\cdot\|$ denotes the Euclidean norm. Figure 6(A) shows the error for the composite-particle approach as a function of the truncation parameters l_{trunc} and κ_{trunc}. The distance between the planar interface and the particle was set to $\Delta z = R$. The best accuracy was achieved for a truncation multipole order of $l_{\mathrm{trunc}} = 25$ and a truncation in-plane wavenumber around $\kappa_{\mathrm{trunc}} = 2.8\,k$. For larger κ_{trunc}, the accuracy drops drastically, because for those in-plane wavenumbers, the point-wise convergency of the PWE has not yet taken place for $l_{\mathrm{trunc}} \leq 30$, compare section 4.1. Interestingly, the best accuracy is not observed for the highest considered SWE truncation order, $l_{\mathrm{trunc}} = 30$, but for $l_{\mathrm{trunc}} = 25$. We suppose that this is because the linear

Optics EXPRESS

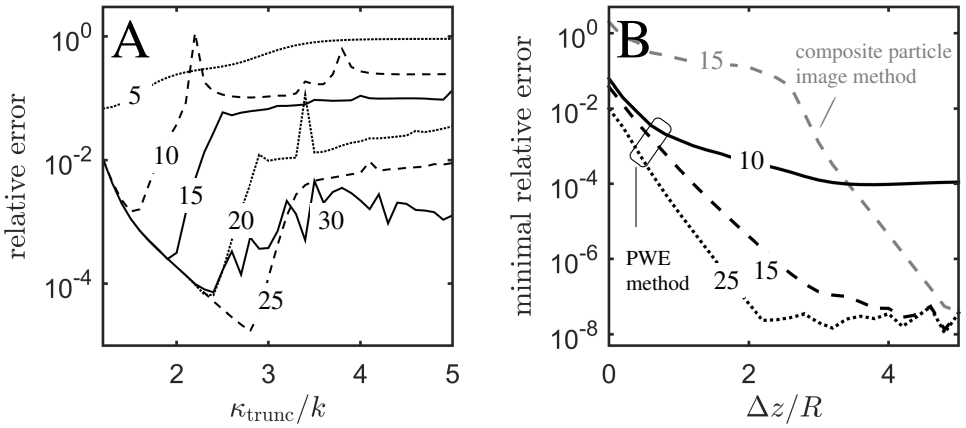

Fig. 6. A) Achieved accuracy as a function of the truncation in-plane wavenumber and truncation multipole order. The distance between the particles and the planar interface was fixed to $\Delta z = R$. B) Minimal error (i.e., for optimal κ_{trunc}), as a function of the distance between the particle centers and the planar interface. The lines refer to different truncation multipole orders (see annotation). The dashed grey line refers to the accuracy that results from the image method for the composite particle for $l_{\mathrm{trunc}} = 15$.

system in Eq. (7) can contain large coefficients and might be ill-conditioned for large l_{trunc}. For the case of light scattering by two overlapping spheres, chaotic behavior with respect to the truncation order of the SWE has been reported [21]. Possibly, the deeper reasons for the here observed instability is related to that issue.

Further, Fig. 6(B) shows the best achieved error (i.e. the minimum with respect to κ_{trunc}) as a function of the particle-substrate distance Δz. If the five spheres touch the substrate, the achievable accuracy for the composite-particle approach is around 10^{-2}. For an increasing distance between the particles and the planar interface the error drops fast and a satisfying accuracy is observed even if the circumscribing sphere of the composite particle significantly intersects the substrate, i.e., for $\Delta z < 4R$. For comparison, we also show the results for the composite-particle approach using the image method, i.e., for solving a two-composite particle problem in free space. Because the circumscribing sphere of the composite particle and its image intersect, the accuracy of that approach is poor for $\Delta z \lesssim 3R$.

5. Second case study: oblate spheroid

The second numerical example is an oblate spheroid with a semi-major axis $A = 250\,\mathrm{nm}$ in the x- and y-direction and a semi-minor axis $C = 50\,\mathrm{nm}$ in the z-direction, located in vacuum above a perfectly conducting substrate with a distance Δz. We consider the cases of a dielectric particle (with a refractive index of 2.4) and of a perfectly conducting particle, see Fig. 7. As before, the system is illuminated from above by a plane wave with unit amplitude, polarized in the y-direction and with a vacuum wavelength $2\pi/k = 550\,\mathrm{nm}$.

The T-matrix for the spheroid is computed by means of the NFM-DS code which is included in [22] and can also be downloaded from [14]. We compute the direct and reflected scattered field $\mathbf{E}_{\mathrm{S}} + \mathbf{E}_{\mathrm{S}}^{\mathrm{R}}$ according to the procedure described in section 2. The SWE truncation multipole order was fixed to $l_{\mathrm{trunc}} = 20$ and for the truncation of the PWE (i.e., of the Sommerfeld integrals) we considered $\kappa_{\mathrm{trunc}} = 3\,k$ and $20\,k$. In an additional simulation, we used the image method (compare [23]) rather than a PWE in order to account for the particle/substrate interaction.

As a reference solution, we used the FEM-based commercial software COMSOL [24] in

Optics EXPRESS

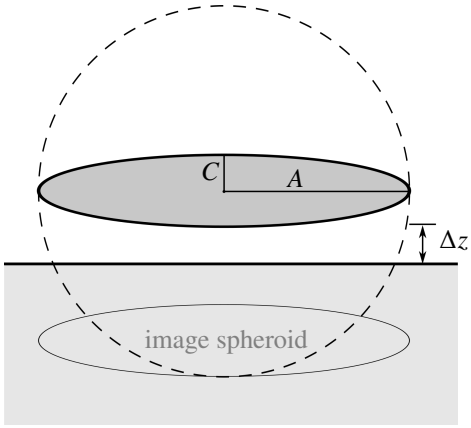

Fig. 7. Oblate spheroid near a perfectly conducting substrate.

order to compute the scattered field. We used the built-in far field projection tool (based on the Stratton-Chu formula) in order to evaluate the far field power flux. The mesh size was selected to provide a good convergence of the far field results.

Figure 8 shows the scattered far field intensity in the xz-plane as a function of the polar angle. For $\Delta z = 300\,\text{nm}$, the circumscribing sphere of the particle does not intersect the substrate. Then, the results of all four computations match very well. However, for $\Delta z = 0$ and 50 nm, the image method does not yield accurate results, because it is based only on the SWE which diverges inside the circumscribing sphere. Likewise, using the T-matrix approach with a rather large Sommerfeld integral truncation order of $\kappa_{\text{trunc}} = 20\,k$ leads to an equally low accuracy. The reason for that can be seen in Fig. 4, where $\kappa = 20\,k$ is well beyond the regime of convergence of the angular spectrum for $l_{\text{trunc}} = 20$, such that the diverging behavior of the SWE affects the results also after the transformation into a PWE. In contrast, the T-matrix results with $\kappa_{\text{trunc}} = 3\,k$ are in good agreement with the reference FEM results for all cases. This again confirms that a smaller truncation scale of the Sommerfeld integrals can result in a higher accuracy.

6. Discussion and conclusions

The T-matrix approach for the computation of the scattered field of a particle near a planar interface can yield accurate results, even if the circumscribing sphere of the particle intersects the planar interface. We have confirmed this claim by theoretical reasoning and numerical examples.

In a related paper, Doicu et al. have already demonstrated that the non-intersection condition can be relaxed up to a certain degree [12]. They pointed out that the smallest sphere containing all singularities of the scattered field's analytic continuation can be smaller than the circumscribing sphere of the scatterer - such that the SWE is (partly) valid inside the circumscribing sphere.

In another previous study, Cappellin et al. [17] emphasized that the plane wave expansion of an antenna in free space is valid in the near field, where the spherical wave expansion diverges.

In the present contribution, we specifically analyzed the convergence mechanism for the case of scattering by oblate particles near interfaces, with a discussion of the transformation properties between spherical and plane vector waves. Mathematically, the coefficients of this plane wave expansion, i.e., the angular spectrum, can be constructed from the spherical wave coefficients by interchanging the order of integration and summation. In practice, this means that for a given truncation multipole order in the T-matrix formalism, the truncation in-plane wavenumber of the plane wave expansion (i.e., the truncation of the Sommerfeld integrals) should be chosen inside the regime where the angular spectrum has converged. Furthermore, increasing the truncation

Optics EXPRESS

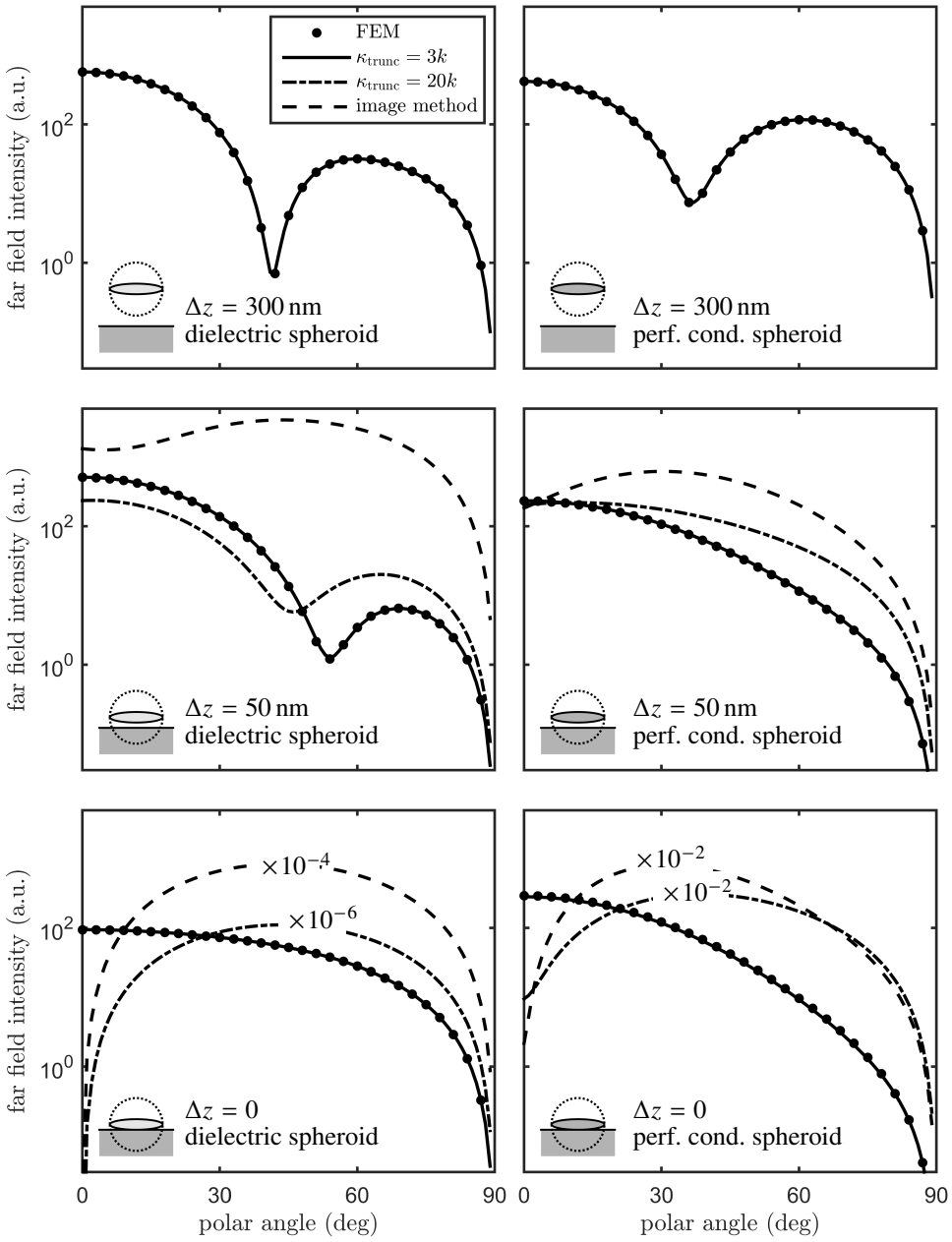

Fig. 8. Scattered far field intensity in the xz-plane as a function of the polar angle for a dielectric ($n = 2.4$, left column) or perfectly conducting (right column) oblate spheroid near a perfectly conducting substrate. The particles are illuminated under normal incidence by a plane wave set at 550 nm. Each row of graphs corresponds to a fixed particle-substrate distance. We compare T-matrix results with a PWE truncation of $\kappa_{\text{trunc}} = 3\,k$ (solid line) and $20\,k$ (dash-dotted line) to FEM results (black dots). In addition, T-matrix results using the image method are shown, too (dashed line). For $\Delta z = 0$, the results for the image method and for $\kappa_{\text{trunc}} = 20\,k$ have been scaled down to fit into the axes box.

Optics EXPRESS

multipole order to very large values again leads to a decrease in the accuracy. We attribute this behavior to an increase in the condition number of the linear system in Eq. (7). The overall achievable accuracy of the scattered field is thus limited for small l_{trunc} by the truncation error and for large l_{trunc} by numerical instability of the linear system. The numerical instability for large l_{trunc} has also been pointed out in [12].

We conclude that the range of applicability of the T-matrix method for the electromagnetic scattering by oblate particles near planar interfaces is larger than one might think from looking at the near field convergency of the spherical wave expansion alone. Instead, the convergency of the plane wave expansion is relevant, and its domain of validity extends into the particle's circumscribing sphere.

The method can be employed for both dielectric and metallic particles or substrates. It is also not restricted to planar interfaces but can be generalized to the scattering by particles near corrugated interfaces [7, 22]. Further, the discussion presented in this paper might also be relevant for the problem of electromagnetic scattering by multiple particles with intersecting circumscribing spheres. In that case, it can be advantageous to compute the particle coupling using a (correctly truncated) plane wave expansion of the scattered field instead of the spherical vector wave addition theorem.

Appendix: Spherical and plane vector waves

The spherical vector wave functions live in the spherical coordinate system (r, θ, ϕ) of the position vector $\mathbf{r}$. We use a similar definition to that given in [22]:

$$\mathbf{M}^{(\nu)}_{lm1}(\mathbf{r}) = \frac{1}{\sqrt{2l(l+1)}} \nabla \times \left(\mathbf{r} z^{(\nu)}_l(kr) P^{|m|}_l(\cos\theta) \, \mathrm{e}^{\mathrm{i}m\phi} \right)$$
$$\mathbf{M}^{(\nu)}_{lm2}(\mathbf{r}) = \frac{1}{k} \nabla \times \mathbf{M}^{(\nu)}_{ml1}(\mathbf{r})$$

The radial wave function $z^{(\nu)}_l$ stands either for the spherical Bessel function of order l, $z^{(1)}_l = j_l$, or the spherical Hankel function of first kind, $z^{(3)}_l = h^{(1)}_l$. Further, $k = n_0\omega/c$ is the wave number and P^m_l denote the normalized associated Legendre functions. The indices of $\mathbf{M}^{(\nu)}_{mlp}$ stand for: p the polarization (TE = 1, i.e. $\mathbf{E} \perp \mathbf{r}$, TM = 2), $m = -l \ldots l$ the angular index with respect to ϕ and $l = 1, 2, \ldots$ the angular index with respect to θ. A multi index n is introduced to subsume them all, $(mlp) \to n$. The number (ν) indicates if the spherical wave is of regular kind ($\nu = 1$) or represents an outgoing wave ($\nu = 3$).

On the other hand, the plane vector wave functions are defined as

$$\mathbf{E}^{\pm}_j(\kappa, \alpha; \mathbf{r}) = \exp\left(\mathrm{i}\mathbf{k}^{\pm} \cdot \mathbf{r}\right) \hat{\mathbf{e}}_j$$

with $(\kappa, \alpha, \pm k_z)$ being the cylindrical coordinates of the wave vector $\mathbf{k}^{\pm}$ for $k_z = \sqrt{k^2 - \kappa^2}$. The plus sign corresponds to waves that propagate / decay in the positive z-direction, whereas the minus sign refers to waves that propagate / decay in the negative z-direction. The index j of $\mathbf{E}_j$ indicates the polarization (1 = TE and 2 = TM). The unit vectors $\hat{\mathbf{e}}_1 = \hat{\mathbf{e}}_\alpha$ and $\hat{\mathbf{e}}_2 = \hat{\mathbf{e}}_\beta$ belong to the azimuthal and polar angle of $\mathbf{k}^{\pm}$, respectively.

The spherical vector wave functions can be expanded in terms of plane vector wave functions and vice versa [20, 22]. We use the relations

$$\mathbf{M}^{(3)}_n(\mathbf{r}) = \frac{1}{2\pi} \int_{\mathbb{R}^2} \mathrm{d}^2\mathbf{k}_\parallel \frac{1}{k_z k} \sum_{j=1}^{2} B_{nj}(\pm k_z/k) \, \mathbf{E}^{\pm}_j(\kappa, \alpha; \mathbf{r}) \, \mathrm{e}^{\mathrm{i}m\alpha} \text{ for } z \gtrless 0 \qquad (11)$$

Optics EXPRESS

and

$$\mathbf{E}_j^{\pm}(\kappa,\alpha;\mathbf{r}) = 4\sum_n \mathrm{e}^{-\mathrm{i}m\alpha} B_{nj}^{\dagger}(\pm k_z/k)\,\mathbf{M}_n^{(1)}(\mathbf{r})\,, \tag{12}$$

where the transformation operator B is given by

$$B_{nj}(x) = -\frac{1}{\mathrm{i}^{l+1}}\frac{1}{\sqrt{2l(l+1)}}\left(\mathrm{i}\delta_{j1}+\delta_{j2}\right)\left(\delta_{pj}\tau_l^{|m|}(x)+\left(1-\delta_{pj}\right)m\pi_l^{|m|}(x)\right) \tag{13}$$

with the spherical functions τ and π defined as

$$\begin{aligned}\pi_l^m(\cos\theta) &= \frac{P_l^m(\cos\theta)}{\sin\theta}\\ \tau_l^m(\cos\theta) &= \partial_\theta P_l^m(\cos\theta)\,.\end{aligned}$$

The matrix $B_{nj}^{\dagger}$ has all explicit i in Eq. (13) set to $-\mathrm{i}$.

Funding

Deutsche Forschungsgemeinschaft (DFG), Priority Program 1839; Helmholtz-Gemeinschaft, Postdoctroal Program; Karlsruhe School of Optics & Photonics; Karlsruhe Institue of Technology (KIT) and DFG, Open Access Publishing Fund.

Acknowledgments

The authors would like to thank Thomas Wriedt and Yuri Eremin for organizing the Bremen workshop on light scattering 2016, and its participants for helpful and encouraging discussions. We thank Philipp Brenner and Jonathan Lehr for proof reading of the manuscript.